ACS APPLIED MATERIALS & INTERFACES

Forum Article

www.acsami.org

Nanocolumnar Structured Porous Cu-Sn Thin Film as Anode Material for Lithium-Ion Batteries

Deniz B. Polat,*[,†] Jun Lu,[‡] Ali Abouimrane,[‡] Ozgul Keles,*[,†] and Khalil Amine*[,‡,§]

[†]Department of Metallurgical and Materials Engineering, Istanbul Technical University, Maslak, Istanbul, 34469, Turkey

[‡]Chemical Sciences and Engineering Division, Argonne National Laboratory, 9700 South Cass Avenue, Argonne, Illinois 60439, United States

[§]Chemistry Department, Faculty of Science, King Abdulaziz University, Jeddah, Saudi Arabia

ABSTRACT: Two nanocolumnar structured porous Cu−Sn films were produced by tuning the duration of the process using an oblique angle deposition (OAD) technique of electron beam coevaporation method. The structural and morphological properties of these porous Cu−Sn films are characterized using thin film X-ray diffraction, scanning electron microcopy (SEM) and atomic force microscopy (AFM). Galvanostatic half-cell electrochemical measurements were conducted in between 5 mV to 2.5 V using a Li counter electrode, demonstrating that the Cu rich Cu_6Sn_5 thin film having homogenously distributed nanocolumns achieved a good cycleability up to 100 cycles with a high capacity retention, whereas the Cu_6Sn_5 nanostructured porous thick film with inhomogeneous morphology showed only a very short cycle life (<25 cycles).The difference in the electrochemical performances of the thin and thick nanocolumnar structured porous Cu−Sn films resulting from different evaporation duration was evaluated on the basis of X-ray photoelectron spectroscopy (XPS) analysis on the cycled samples.

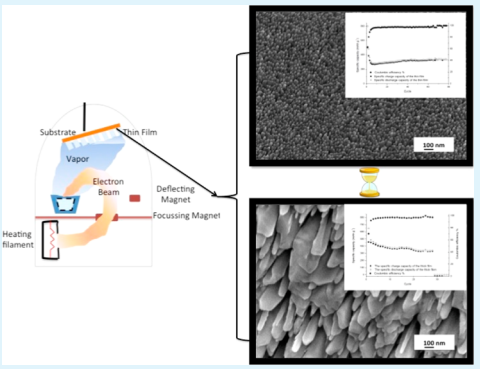

KEYWORDS: *anode, porous thin film, inclined nanocolum, oblique angle deposition, lithium-ion battery, electron beam*

1. INTRODUCTION

Recently, research has been focused on developing new anode materials with higher reversible capacity than the conventional carbon-based materials. Metals, metal alloys, and intermetallic compounds have been investigated as negative electrodes for lithium-ion batteries.[1−5]Among them, tin has been widely studied because it has a higher theoretical capacity (994 mAh/g) compared to graphite (372 mAh/g).[6] However, the use of pure tin as anode is limited because of its significant volume change during lithiation/delithiation processes, which led to severe pulverization of the anode and, thus, rapid capacity fade.[7]

Several strategies have been proposed to overcome this volume fluctuation during cycling, including optimization of the electrode composition as well as the morphology of the electrode. For instance, Huggins et al.[7] reported the use of an inert matrix along with active metallic tin in order to achieve high performance of the anode materials. Besenhard et al.[3,8,9] and Yang et al.[10] further investigated the use of metallic tin alloys as anode material, where inactive metals act as a buffer to absorb the high volume changes during the cycling. Among these tin alloy systems, Cu−Sn intermetallic compounds have been proposed as alternative anode materials for lithium ion batteries due to their strong structural integrity between the parent binary Cu−Sn intermetallic electrodes with their lithiated products.[11,12] In addition, the Cu−Sn intermetallic compounds are relatively inexpensive and environmentally friendly.[13] For example, Cu_6Sn_5 demonstrated a much longer cycle life compared to that of the pure Sn. During lithiation, Li^+ first reacts with Cu_6Sn_5 to form $Li_xCu_6Sn_5$ (eq 1). Further addition of Li^+ to $Li_xCu_6Sn_5$ leads to the phase segregation of the lithiated compound into $Li_{3.5}Sn$ alloys (eqs 2 and 3) that is surrounded by Cu matrix.[8,14] The formation of Li_7Sn_2 ($Li_{3.5}Sn$) in the lithiated compound was demonstrated justified by Mössbauer spectroscopy and TEM analyses results[15,16]

$$x\mathrm{Li} + \mathrm{Cu_6Sn_5} \rightarrow \mathrm{Li}_x\mathrm{Cu_6Sn_5} \quad (1)$$

$$(10 - x)\mathrm{Li} + \mathrm{Li}_x\mathrm{Cu_6Sn_5} \rightarrow 5\mathrm{Li_2CuSn} + \mathrm{Cu} \quad (2)$$

$$3\mathrm{Li} + 2\mathrm{Li_2CuSn} \rightarrow 2\mathrm{Li_{3.5}Sn} + 2\mathrm{Cu} \quad (3)$$

As a consequence, ductile and electrical conductive Cu enhance the electrochemical performance of the Cu−Sn anode, as evident by the longer cycle life observed. Nanoscale Cu_6Sn_5 powders,[17] a binder-free 3D porous Cu_6Sn_5 anode,[18] a sputtered-deposited Cu_6Sn_5 thin film,[19] and electrochemically assisted Cu_6Sn_5 nanocolumns[20,21] have been fabricated and tested as the anode material for Li-ion batteries, all of which showed significantly improved electrochemical performance. In

Special Issue: New Materials and Approaches for Electrochemical Storage

Received: December 27, 2013
Accepted: March 25, 2014
Published: April 8, 2014

particular, Cu_6Sn_5 with nanocolumnar structure showed a great potential to be used as an anode in lithium-ion batteries because it can avoid the particle−particle interaction which causes "the electrochemical sintering" of nanosized particles during electrochemical cycling otherwise. In addition, the free space between the nanocolumns creates an easy access for the electrolyte to the entire surface and accommodates the volume changes during the lithiation/delithiation. As a result, nanocolumnar Cu_6Sn_5 is expected to provide a high capacity retention to the electrode, and therefore, a longer cycle life.

Under a condition of an obliquely incident flux, thin film with a nanocolumnar structure can be fabricated using physical vapor deposition method. This technique is so-called Oblique Angle Deposition (OAD). This method becomes remarkable among its alternatives because it can avoid the hazardous handling of flammable, explosive or cancerogenous metal nanoparticles. In addition, OAD enables direct deposition of the well-aligned inclined nanocolumns on the current collector, eliminating the need of binder or conductive additives to get homogeneously distributed porosities, which ensures the direct transportation of the electrons; hence a fast Li^+ diffusion through their adjustable, small diameters.[22]

Karabacak et al.[23] studied the mechanism of the nanocolumns formation during the OAD method. Their results indicate that it is possible to control the orientation of the column growth by changing the incident flux angle under low pressure because the electron beam deposition is a line-of-sight process. Therefore, the columns are formed when the evaporated particle flux strikes to the substrate under a highly oblique angle (normally, $\theta \geq 80°$). Karabacak et al.[23] also pointed out that the dominated mechanisms that control the oblique angle deposition are self-shadowing at the atomic scale and the surface diffusion process. At room temperature deposition, since the surface diffusion rate is very slow, once the adsorbed atoms nucleate on active sites of the substrate surface, they tend to grow as inclined nanocolumns if such growth is governed by Volmer−Weber or Stranski−Krastanov process. In this case, factors such as surface roughness of substrate, process duration and evaporation source composition have significant impact on the composition and the architecture of the produced thin films, which are expected to further affect their electrochemical performances.[24]

The objective of the current study is to use the OAD method as an alternative production technique to form nanocolumnar Cu−Sn thin film on Cu foils, and optimize the evaporation duration to form a homogeneous Cu−Sn film with porous nanocolumnar structure. The OAD is performed on a stationary substrate with a fixed position at 80° (fixed incident angle) at room temperature. Such Cu−Sn intermetallic compound with unique nanostructure is expected to exhibit enhanced performance when used as anode in rechargeable lithium-ion batteries. The difference in the electrochemical performances of the nanostructured thin films with different thickness is also discussed on the basis of the electrochemical measurements and XPS results.

2. EXPERIMENTAL SECTION

Two nanocolumnar structured porous thin (<250 nm) and thick Cu−Sn (between 250 nm to 1 μm) films are deposited on chemically polished (8 wt. H_3PO_4 electrolyte) Cu discs (15.5 mm diameter and 1.5 mm thickness) using an electron beam deposition technique at different process durations (45 min and 90 min, respectively). The deposition of porous nancolumnar Cu−Sn films on Cu substrate is realized by the coevaporation of Cu and Sn pellets. The pellets are present together in a graphite crucible prior to deposition process. Cu:Sn weight ratio in the crucible is 1:1.

First, a flat Cu−Sn film is deposited with an incident angle of 0° to enhance the electronic contact, to reduce the ohmic resistance and thereby to delay aggregation in the electrode during cycling.[25] During the discharge reaction, the nonporous layer with a Li concentration gradient provides a gradual transition to current collector and eliminates the stress "singularity" at the current collector interface. Therefore, more adherent coating is achieved, which in turn results in long cycle life during galvanostatic test. After the nonporous layer, then, the inclined Cu−Sn nanocolumns are formed on top of it, when the deposition flux hits onto the substrate surface with an angle of 80° at the room temperature. Taking the advantage of the shadowing effect and the limited adatom diffusion, the inclined nanocolumns are formed with homogenously distributed nanosized porosities among them. The deposition flux (4 Å s^{-1}) and the substrate temperature (around 30 °C) are constant during the overall process and the base pressure in the vacuum chamber is 1×10^{-7} Torr. A stainless steel (15.6 mm diamater) and pure silicon wafer (20×10 mm^2) are also coated under the same deposition condition, which enables us to make compositional analyses and measure the coating thicknesses accurately.

The compositions of the deposited Cu−Sn films are determined by energy -dispersive X-ray spectroscopy (EDS) analysis. The weight of the thin films is measured by using a microbalance before and after the coating process (Myweight i101). The surface morphology and thickness of the films are investigated by utilizing field-emission scanning electron microscopy (FE-SEM, JEOL JSM 7000F). The surface roughness of the films prior to electrochemical analyses is also determined via AFM (with Digital Instrument (DI) Controller IV under dimension 3100 platform). The phases present in the coatings are determined using a thin film XRD (Philips PW3710 System) with a 2θ range of 20−90° in steps of 0.05°(with CuKα at 40 kV and 30 mA).

To determine the change in the composition and the chemical state of the samples formed at different evaporation durations, we performed X-ray photoelectron spectroscopy (XPS) analyses using a Kratos Axis Ultra DLD surface analysis instrument, on the pristines, the first discharged and the first charged samples. Prior to introduction into the load-lock vacuum chamber of the XPS instrument, all air-sensitive samples were loaded into an inert transfer module interfaced with the instrument. Samples were prepared in an Ar-filled glovebox, with no more than 1 ppm O_2 and 1 ppm H_2O. The base pressure of the analysis chamber during these experiments is 3×10^{-10} Torr, with operating pressures around 1×10^{-9} Torr. Spectra are collected with a monochromatic Al Kα source (1486.7 eV) and a 300×700 μm spot size. Peak position correction is further corrected by referencing the C 1s peak position of the adventitious carbon for a sample (284.8 eV, PHI Handbook of Photoelectron Spectroscopy), and shifting all other peaks in the spectrum accordingly. Fitting is done by using the program CasaXPS. Each relevant spectrum is fit to a Shirley type background to correct for the rising edge of the backscattered electrons that shift the baseline higher at high binding energies. Peaks are fit as asymmetric Gaussian/Lorentzians, with 0−30% Lorentzian character.

To evaluate the electrochemical performances of the nanostructured composite electrodes, their electrochemical behaviors versus $Li/Li^+$are examined using a conventional two-electrochemical system. Test cells are prepared in an argon filed glovebox (MBRAUN, Labmaster) based on the following sequence: (i) a working electrode; (ii) a 1 M $LiPF_6$ in the ethylene carbonate-dimethyl carbonate, EC:DMC 1:1 (Merck Battery grade) electrolyte solution; (iii) a separator (Celgrad 2400) and iv) a lithium metal foil as the counter electrode. The cells are tested at the room temperature in between 5 mV to 2.5 V versus Li/Li^+ under a current density of 50 mA g^{-1}. Cyclic voltammetry (CV) is performed in the potential range of 5 mV to 2.5 V versus Li/Li^+ at a scan rate of 0.03 mV s^{-1} and EIS analyses are accomplished in a frequency range 10 mHz to 10000 Hz (Gamry pci4/750).

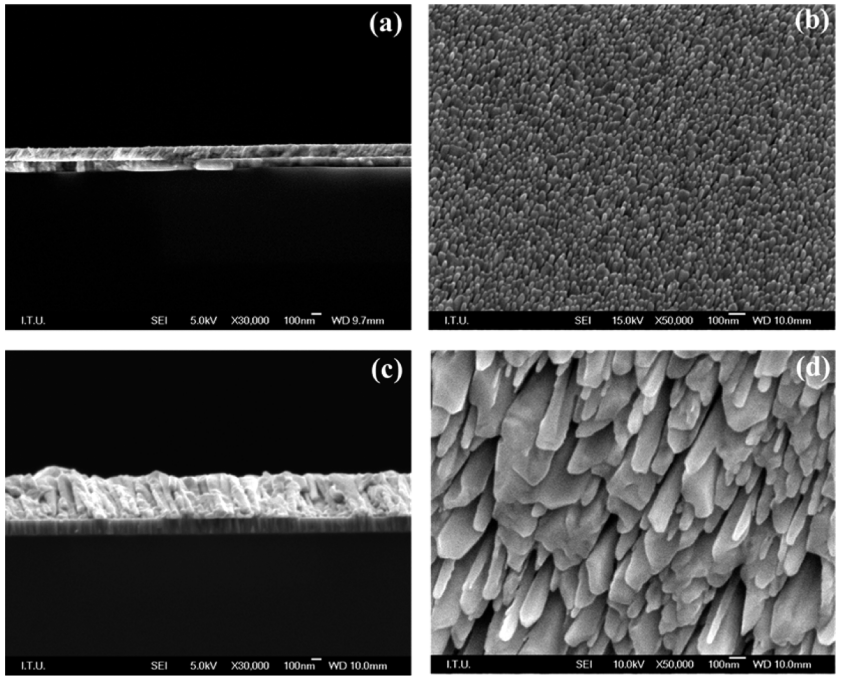

Figure 1. FE-SEM images of (a) surface, (b) cross-section of the nanocolumnar structured porous Cu−Sn thin film; (c) surface, (d) cross-section of the Cu−Sn thick film.

3. RESULTS AND DISCUSSION

3.1. Effect of Evaporation Duration on the Morphological and the Structural Properties of the Nanocolumnar Structured Porous Cu−Sn Films. In OAD methods, when Cu−Sn vapor atoms are deposited on the substrate, the atomic shadowing and the limited adatom diffusion functionalize together to produce a microstructure of small isolated columns. During the deposition, there is a strong competition and extinction effect among these nanocolumns, which leads to inhomogeneity of the thin film morphology in the plane parallel to the substrate, even the competition among columns urges the film to be uniform in the direction along the substrate's surface normal.[26,27] This competition becomes more severe as the process duration increases. Figure 1a−d demonstrates that an increase in the evaporation duration may affect the balance between the atomic shadowing and adatom diffusion processes, which in turn distorts the homogeneous morphology of the film and increases the film thickness from 230 to 600 nm. This can be interpreted by "the broadening" process, which is commonly observed for the microstructural defects, detected in the OAD thin films when the thickness of the film is increased.[23]

The surface morphology was further analyzed by AFM (Figure 2a, b), which showed that prolonging the process duration of OAD leads to a higher surface roughness (i.e., 8.27 nm for thick and 4.85 nm for thin porous film). As mentioned earlier, the evaporated atoms nucleate on the active sites of the substrate in the form of small islands and the subsequent growth occurs on the previously formed nuclei during the OAD process. An increase in the evaporation duration enhances the surface energy of the deposited grains, which tends to be reduced by forming agglomerates on the highly active sites of the electrode surface, forming an inhomogeneous size distribution of columns in the nanostructured thick film. Therefore, extending the evaporation duration promotes the direct growth of the inclined nanocolumns with a higher surface roughness, as demonstrated by AFM analyses.

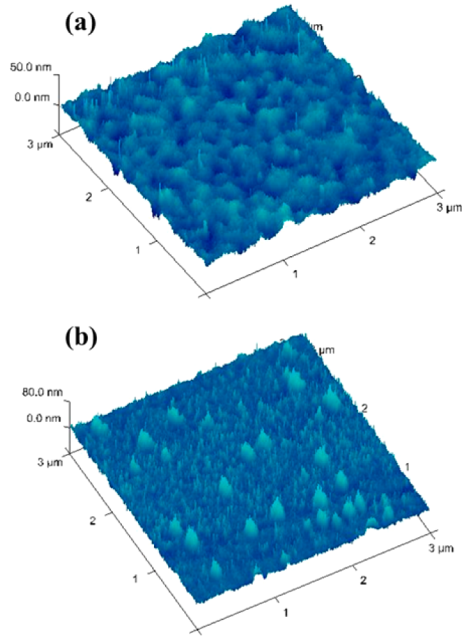

Figure 2. AFM images of (a) thin, (b) thick nanocolumnar structured Cu−Sn porous films.

The chemical composition and structure of the samples are investigated by thin-film XRD technique, as shown in Figure 3. The results reveal that the thin porous film consists of copper rich Cu_6Sn_5 phase ($Cu_{6.26}Sn_5$), whereas the thick porous film contains stoichiometric Cu_6Sn_5 phase. Using the Rietveld refinement method, calculated lattice parameters for $Cu_{6.26}Sn_5$ in reference to Cu_6Sn_5 are found as *a*, 4.23 Å, *c*, 5.14 Å and a, 4.22 Å, *c*, 5.10 Å, respectively. The excess of copper in Cu-rich Cu_6Sn_5 phase in thin porous film causes the small shifts at high

dx.doi.org/10.1021/am405994b | ACS Appl. Mater. Interfaces 2014, 6, 10877−10885

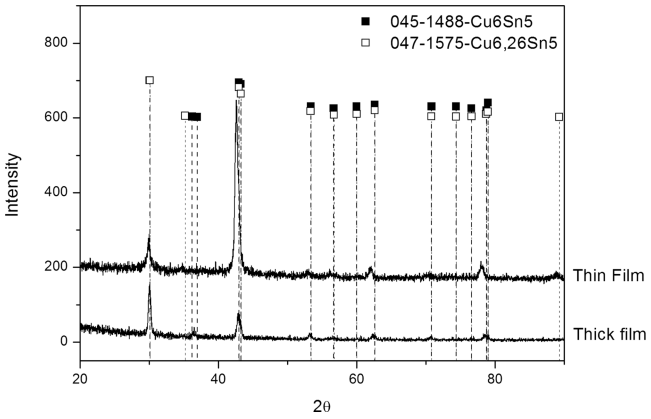

Figure 3. XRD patterns of nanocolumnar structured thin and thick porous Cu−Sn films.

diffraction angles due to the internal stress into Cu_6Sn_5 crystal. The existence of the excessive copper in the thin porous film is also confirmed by EDS analyses (Table1), numerically. Table 1

Table 1. EDS Analyses of Thin and Thick Porous Cu−Sn Films

thin film		thick film	
Cu (at %)	Sn (at %)	Cu (at %)	Sn (at %)
67.87	32.13	52.05	47.95

shows that the film composition changes depending on the evaporation duration, even both films are formed as a result of Cu−Sn coevaporation from one crucible having the same composition before evaporation. Considering that the evaporation temperature of both metals are very close to each other under high vacuum and the evaporation is performed through one crucible where the Cu:Sn ratio (1:1 weight ratio) is fixed prior to the OAD process, the evaporation rate of copper is faster than that of tin, because the density of copper and tin are 63.5 and 118.71 g mol^{-1}, respectively. Thus, at an early stage of the evaporation, Cu-rich phase forms on the substrate surface due to the high number Cu atoms present in the crucible. As the evaporation process continues, the number of Cu atoms decreases in the crucible, which favors the evaporation of tin pellets in long process duration forming stoichiometric Cu_6Sn_5 nanocolumns in the thick film.

3.2. Effect of Evaporation Duration on the Electrochemical Performances of the Nanocolumnar Structured Porous Cu−Sn Films. Figures 4a and b show the Cyclic Voltammogrames (CV) of the porous thin and thick Cu−Sn films. Similar reduction peak for the formation of Li−Sn compounds and similar anodic peaks corresponding to Li dealloying reactions from Sn are detected for both samples.[16]

Copper-rich Cu−Sn ($Cu_{6.26}Sn_5$) thin film has a sharp reduction peak at 5 mV in addition to numerous peaks between 0.2 and 0.4 V. However, the thick film with stoichiometric Cu_6Sn_5 has one sharp reduction peak at 5 mV and one broad reduction peak around 0.25 V. These cathodic peaks are related to the presence of intermetallic phases formed during Li^+ insertion into the Cu−Sn films. According to Shin et al.,[16] the reduction peaks around 0.3 V can be attributed to the formation of Li_2CuSn from Cu_6Sn_5 (Reaction 1) and peak at 5 mV shows clearly the formation of fully lithiated phase from Li_2CuSn (Reactions 2−3). Our results prove that the

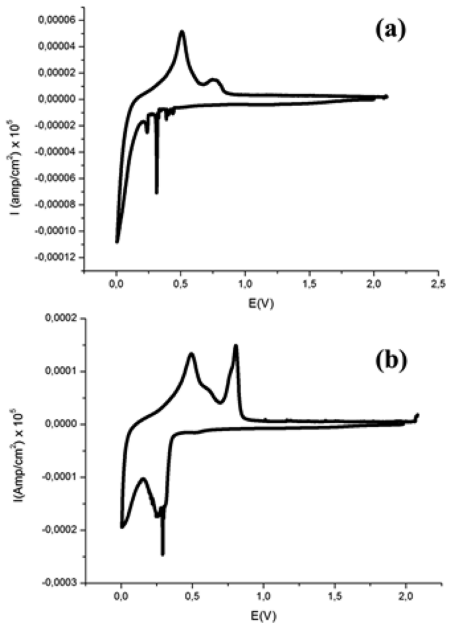

Figure 4. CV of the as-deposited nanocolumnar structured porous (a) thin, (b) thick Cu−Sn films.

evaporation duration does not affect the reaction mechanism of the Cu−Sn films since Cu has no reaction with Li. For the anodic peaks, the Cu-rich Cu−Sn thin film has one sharp peak at 0.5 V and one broad peak around 0.6−0.8 V, whereas the thick film with Cu_6Sn_5 has two peaks at 0.5 and 0.8 V. Moreover, the thick film has a small anodic peak at 0.6 V. These anodic peaks correspond to the recovery of Li_2CuSn from Li_7Sn_2 and Cu_6Sn_5 from Li_2CuSn, respectively.[16]

Figures 5a-b show the voltage versus the specific capacity curves for the porous Cu−Sn films with different thicknesses. The voltage profiles of both films are similar to that of pure tin, which indicates that the deposited Cu−Sn films have similar reaction mechanism during lithiation/delithiation compared to that of the pure tin. In other words, the alloying-dealloying of Li with Sn is independent of the evaporation duration and the composition of these films. In the initial discharge curves of both electrodes, voltage drops to 0.3 V immediately after starting the test then stabilizes, and decreases again gradually down to 0.02 V, which corresponds to the formation of $Li_{3.5}Sn$.[15,16,28,29] For Cu−Sn thick film electrode, the voltage plateaus are not noticeable because the presence of a substantial amount of copper hinders the formation of Li−Sn phases. Panels a and b in Figure 5 also demonstrate that the SEI layer forms around 0.3−1.0 V, counting for the major reason of the irreversible capacity loss for the first cycle of the films. The SEI formed on the porous Cu−Sn films seems to be stable since the charge consumption in 0.2−1.2 V in the following cycles is drastically reduced with 97% Coulombic efficiency. (see Figure7).

To further examine the electrochemical behaviors of the porous nanocolumnar Cu−Sn films, we compared the impedance data of each cell after the first and the 25th cycles in panels a and b in Figure 6. EIS spectra of the thin and thick Cu−Sn films after first discharge−charge cycle show one and two semicircles at the high frequency region, respectively (Figure 6a, b). It has been reported that the first semicircle is associated with SEI formation; while the second semicycle provides information about the transport of the adsorbed

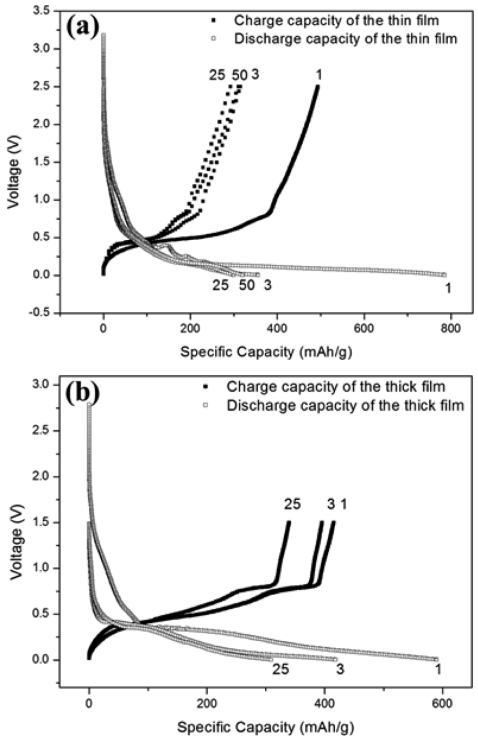

Figure 5. Voltage versus specific capacity curves for nanocolumnar structured (a) thin and (b) thick porous Cu−Sn films.

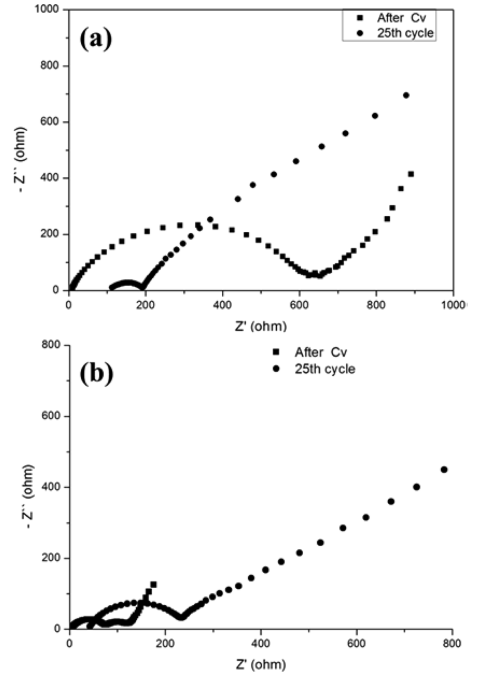

Figure 6. Electrochemical impedance spectroscopy for nanocolumnar structured (a) thin and (b) thick porous Cu−Sn films after the 1st and the 25th cycles.

species along the structure and the upward slope at the low frequency demonstrates the Li^+ diffusion through the bulk material.[30] When EIS data of each film is observed a very low initial ohmic resistance is noted, proving that the interface between the coating and the current collector is well established. Figure 6a shows that a decrease in the arc diameter of the semicircle in the high frequency region and an increase in the ohmic resistance of the cell are remarkably noted for the (Cu-rich) $Cu_{6.26}Sn_5$ thin film. This change in the impedance at the charge transfer interface is likely due to the SEI formation followed by the pulverization and the partial delamination of the film, resulted from the volumetric changes occurred in cycling.[19] It should be noted that after the first cycle, the homogeneous $Cu_{6.26}Sn_5$ nanocolumns with a high surface area leads to a high impedance on its EIS spectra because of the SEI formation. As lithiation/delitahiation occurs, a partial delamination happens followed by pulverization of the film on the remaining part of the electrode. Thereby due to the partially lost of contact of the film with the current collector the contact resistance is increased in the spectra, and he SEI resistance is decreased. Thus, a better capacity utilization occurs on the remaining part of the anode, resulting in a high Coulombic efficiency (Figure 7a). For the thick nanocolumnar Cu−Sn

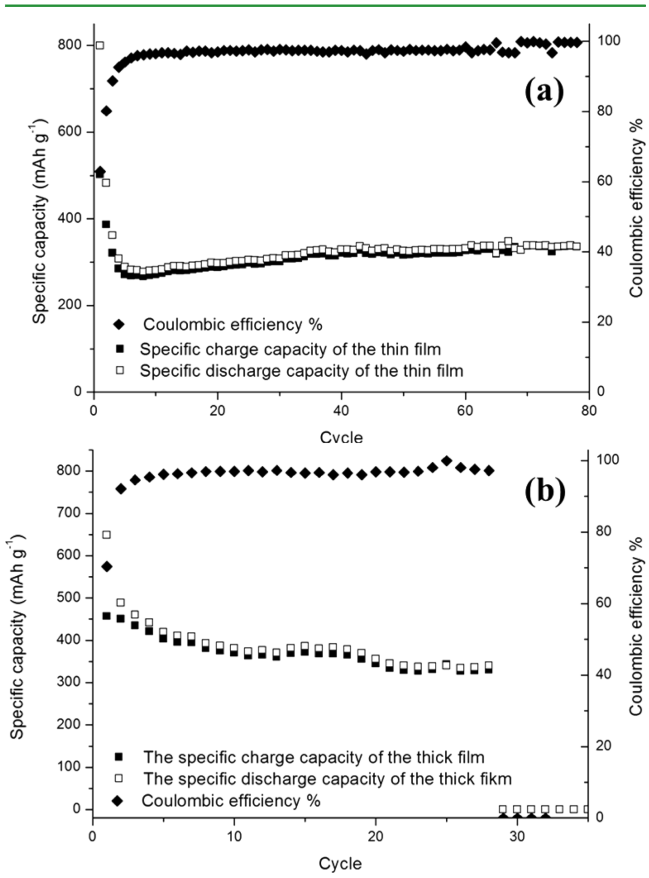

Figure 7. Discharge capacity, charge capacity and Coulombic efficiency are plotted as a function of cycle numbers for (a) thin and (b) thick Cu−Sn porous films.

porous film, the comparison between the first and 25th cycles EIS data reveal that rough electrode surface results in formation of two semicircles (proving multiple contact of the thin film with the electrolyte) in the high frequency region. At 25th cycles, two semicircles immerge together, where a higher contact resistance is noted eventually (Figure 6b).

Here in, the formation of the SEI layer on the electrode surface appears to be crucial to the electrochemcial performance of the cells. Therefore, we apply the XPS technique to demonstrate the difference of the SEI formed on the thin and thick films and study how these SEI affect the cell perfromance. Figures 8 shows the XPS spectra of pristine, first discharged and

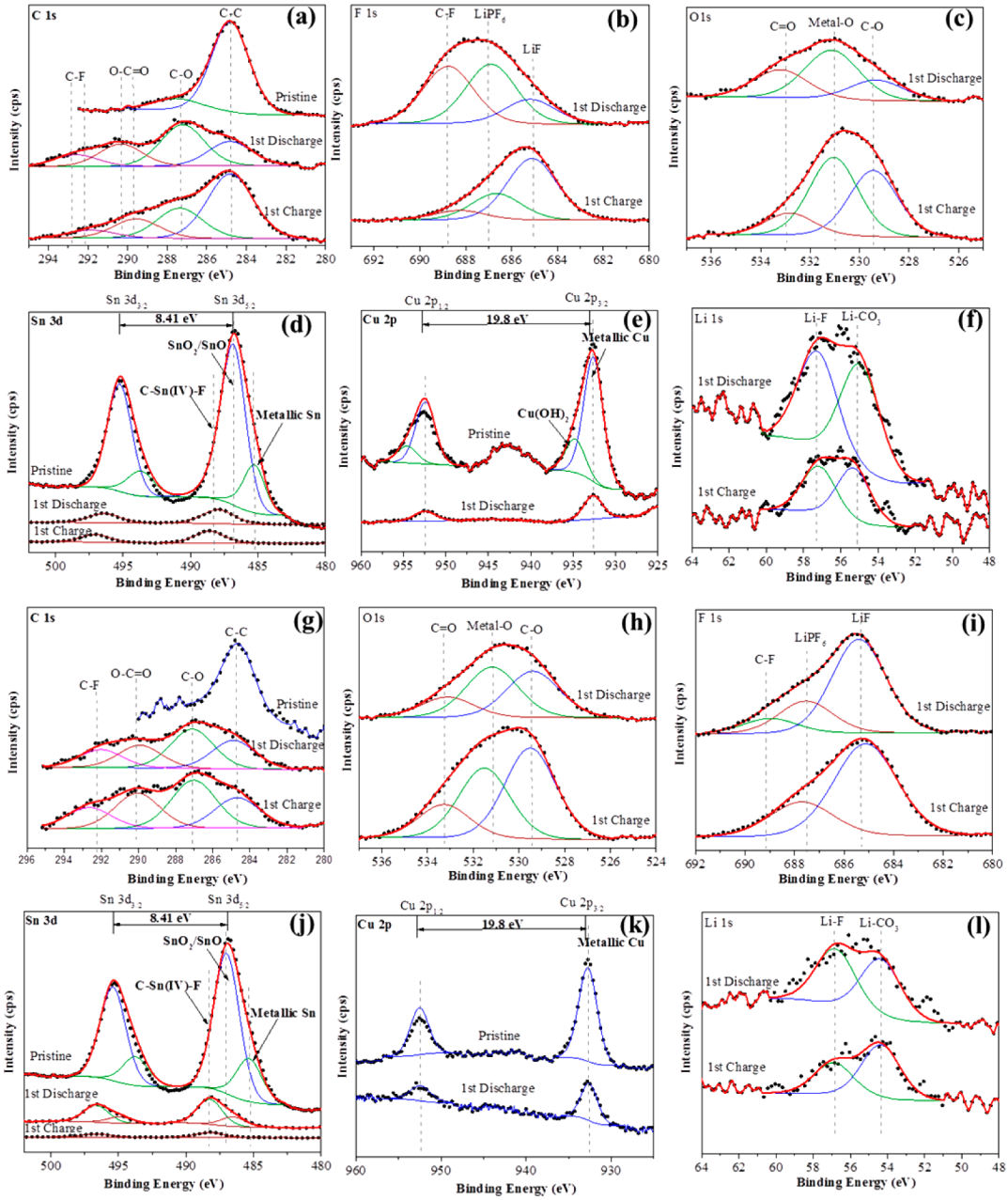

Figure 8. XPS spectra of C1s, O1s, F1s, Sn 2p, Cu 2p, and Li 1s of (a–f) thin film and (g–l) thick film, respectively, as pristine, after thefirst discharge and the first charge process.

first charged samples of both thin and thick electrodes. Because XPS is a surface sensitive analysis, the results demonstrate the changes in the surface composition at the electrode (or SEI)-electrolyte inerface. The absence of binder in these anodes allows more straightforward analysis of SEI formation and changes in anode surfaces.

The XPS spectra of these anodes suggest changes in the electrode surface properties after the first discharge and charge reactions (Figures 8). Except for the C1s peaks associated with the universal contamination, Sn, SnO_x (SnO/SnO_2) and Cu metallic peaks are also detected on the pristine (as-deposited) electrodes. In addition, $Cu(OH)_2$ species is also detected on thick film. SnO/SnO_2 peak presents on the surface of both pristine electrodes, resulting from the contact with air. SnO_x could be a possible reason for the low Coulombic efficiency observe at the first cycle, because it will go through an irreversible reaction with lithium during the first lithiation reaction. When the first discharged samples of both thin films are investigated in detail, XPS analyses reveal no existence of metallic Sn peaks. Small amounts of metallic Cu and C–Sn(IV)–F peaks can be identified on both films. XPS analyses also show Li–F, C–F, $Li–CO_3$, O–C═O, C–C, C═O, and M–O peaks on both discharged samples, where M could stand for Sn in that case.

Upon charging, C–C, C–O, C═O peaks justify the presence of SEI layer on both charged samples and XPS data shows that Sn is present in these oxide films as C–Sn(IV)–F form. C1s peaks detected around 285.5–289 eV (C–C, C–O and O–C═O) might associate with the presence of PEO (polyethylene oxide) or ether functionalities or lithium alkoxides formed on charged anode material.[30] These compounds could be derived from a one electron reduction

of DEC or EC or carbonate, which are further reduced to form ether, alkoxide, ester, carboxylate, and lithium oxide products of the SEI present on the anode material.

Our XPS results (Figure 8) are similar to those previously reported[30,31] for Sn-based thin film anode material and reveal that SEI is primarily composed of electrolyte reduction products. We also noted that metallic Sn start to be formed on the anode surface after the first discharge process. The amount of Cu in the thin film seems to have no effect on SEI formation since it is an inactive metal with Li, hence, it is possible to consider the role of Cu on electrochemical performance of anodes mostly for its buffering effect.

The XPS results are in good agreement with the results from the electrochemical analyses (Figures 4a-b, 6a-b). They all demonstrate that the SEI composition is independent of the thin film thickness and the Cu content in the thin film; but it depends mostly on the electrolyte concentration and the types of additives. In our study, the XPS data of both electrodes are similar because we use $LiPF_6$-EC based electrolyte. Once SEI forms, with its "glue effect", it prevails on the electrode in subsequent cycles and suppresses the lost of contact among small Sn particles generated from the high volume changes. Nie et al.[32] observed the similar SEI formation on the anode surface after several cycles by TEM analyses, which supports our observation. The SEI formation continues to evolve on the electrode for first few cycles and gathers Sn nanoparticles together,[32] if there is enough space in the electrode to mechanically tolerate the volume changes in the thin film.

Figure 7 shows the specific capacity−cycle curves of the porous nanocolumnar Cu−Sn films having different thicknesses. The capacity value in the graph is calculated based on the active material present in the thin film. The capacity of the porous Cu-rich Cu−Sn thin film (784.7 mAh g^{-1}, discharge capacity) exceeds the theoretical capacity of Cu_6Sn_5 thin film (608 mAh g^{-1}, discharge capacity)[33] and other Cu−Sn anodes previously fabricated and tested in literature.[34−36] This might be interpreted by the formation of SEI layer or the presence of SnO_x phases on the thin film electrode surfaces, as stated earlier. A decrease in the capacity is observed up to third cycles; since then, the decay in the capacity of the thin film disappears and the capacity increases slightly in the later cycles (up to 40 cycles). The low capacity fading observed for the thin film might be attributed to the architecture of the thin film electrodes. It is convincible that some of the Cu−Sn particles (on nonporous layer), which are isolated from the electrolyte at the beginning, may become active as the electrolyte penetrates through the pores with cycling. After 40th cycle, the increase in capacity seems less pronounced (Figure 7a), and the anode performs approximately 300 mAh g^{-1} with a high cycle retention (99.5% Coulombic efficiency) even after 100cycles. Figure 7b demonstrates that the initial discharge capacity of the thick porous Cu−Sn film is lower than that of the Cu-rich porous Cu−Sn thin film. It might be caused by the limited Li^+ diffusion into thick film due to the inhomogeneous geometry (columns and pores with different diameters). Moreover, unlike the thin film's initial Coulombic efficiency (62%), the thick film gives a higher initial Coulombic efficiency (90%) which is explained by the preferential orientation of Li in the thick film during cycling. The unhomogeneous morphology forming limited accessible surface area for Li^+, favors the travel of Li^+ among those porosities during the first cycle. Even the thick porous film exhibits a higher first cycle Coulombic efficiency (90%), its cycle life is very short (28 cycles). It is still not clear that why the thick film electrode fades so quickly. However, it is possible that the inhomogeneous column size distribution with high Sn content of the thick film could account for its low cycle life because high volume changes during the lithium insertion−deinsertion could not be recovered mechanically from the electrode, even though SEI tried to keep the electrode with its glue effect.

SEM analysis was also conducted for both samples after the first cycle to reveal their surface morphology changes. Figure 9a shows that after the first cycle, the morphology of the homogeneous nanocolumnar thin film is changed, where a decrease in particle size is clearly noted. On the other hand, a remarkable delamination of the film from the current collector is observed for the thick film after the first cycle, as shown in Figure 9b. The inhomogeneous morphology of the thick film resulting from the prolonged evaporation duration seems to cause a short cycle life because the agglomerated particles in the electrode cannot tolerate the volumetric change homogenously.

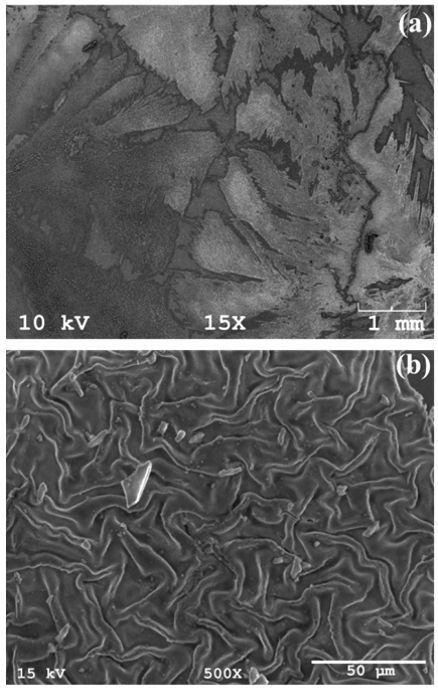

Figure 9. FE-SEM images of the nanocolumnar structured porous (a) thin, (b) thick Cu−Sn films after the first cycle.

4. CONCLUSIONS

In this study, by changing the evaporation duration, porous nanocolumnar structured Cu−Sn films with different thicknesses are produced via OAD method. The morphological and compositional analyses results show that long evaporation duration leads differences in Sn contents and morphologies of both films, which appear to have significant impact on their electrochemical performances when used as anodes for lithium ion batteries. The thin film having ordered nanocolumns exhibits a a high initial discharge capacity (784.7 mAh g^{-1}) with 40% Columbic efficiency. The Coulombic efficiency becomes 99.5% at 100th cycles where 300 mAh g^{-1} capacity is delivered by the thin film electrode. Thirty-eight percent of the initial discharge capacity is retained after 100 cycle for the thin film because of the presence of its well-aligned nanocolumns made of nanosized particles. In fact, nanoparticle presence in these

nanosized columns and homogeneous distribution of porosities among these columns facilitate Li^+ diffusion within the thin film. The additional amount of Cu increases the ductility and the conductivity of the thin film which increases the stress tolerance of the electrode against the volumetric change occurred during lithiation/delithiation processes. On the other hand, the thick porous Cu_6Sn_5 anode fades after 25 cycles, although it shows a high Columbic efficiency (99.5%). The prolonged evaporation duration seems to cause the instability of the electrode and short cycle life due to the inhomogeneous morphology of the anode, forming a highly rough surface. XPS analyses show that the SEI composition depends only on the electrolyte and the active material in the thin film.

AUTHOR INFORMATION

Corresponding Authors

*E-mail: bpolat@itu.edu.tr. Tel: 0090 212 285 3398.
*E-mail: ozgulkeles@itu.edu.tr.
*E-mail: amine@anl.gov. Tel: 630-252-3838.

Notes

The authors declare no competing financial interest.

ACKNOWLEDGMENTS

This work is a part of the research project 110M148 approved by The Scientific and Technological Research Council of Turkey (TUBİTAK). The research grant is gratefully acknowledged. This work was also supported by the U.S. Department of Energy under Contract DE-AC0206CH11357 with the main support provided by the Vehicle Technologies Office, Department of Energy (DOE), Office of Energy Efficiency and Renewable Energy (EERE). J. Lu was supported by the Department of Energy (DOE) Office of Energy Efficiency and Renewable Energy (EERE) Postdoctoral Research Award under the EERE Vehicles Technology Program administered by the Oak Ridge Institute for Science and Education (ORISE) for the DOE.

REFERENCES

(1) Lee, K. H. Si Nanowires for an Anode Material of Li Batteries. *Ph.D. Thesis*, Pohang University, Korea, 2007.

(2) Wachtler, M.; Besenhard, J. O. Tin and Tin-Based Intermetallics as New Anode Materials for Lithium-Ion Cells. *J. Power Sources* **2001**, *94*, 189−193.

(3) Besenhard, J. O.; Yang, J.; Winter, M. Will Advanced Lithium-Alloy Anodes Have a Chance in Lithium-Ion Batteries ? *J. Power Sources* **1997**, *68*, 87−90.

(4) Kamali, A. R.; Fray, D. Tin-Based Materials as Advanced Anode Materials for Lithium Ion Batteries: a Review. *J. Rev. Adv. Mater. Sci.* **2011**, *27*, 14−24.

(5) Lindsay, M. J.; Wang, G. X.; Li, H. K. Al-Based Anode Materials for Li-Ion Batteries. *J. Power Sources* **2003**, *119*, 84−87.

(6) Kumar, T. P.; Ramesh, R.; Lin, Y. Y.; Fey, G. T. K. Tin-Filled Carbon Nanotubes as Insertion Anode Materials For Lithium-Ion Batteries. *Electrochem. Commun.* **2004**, *6*, 520−525.

(7) Deng, D.; Kim, M. G.; Lee, J. Y.; Cho. Green Energy Storage Materials: Nanostructured TiO_2 and Sn-Based Anodes for Lithium-Ion Batteries. J. *Energy Environ. Sci.* **2009**, *2*, 818−838.

(8) Besenhard, J. O.; Komenda, P.; Paxinos, A.; Wudy, E.; Josowicz, M. Binary and Ternary Li-Alloys as Anode Materials in Rechargeable Organic Electrolyte Li-Batteries. *Solid State Ionics* **1986**, *18−19*, 823−827.

(9) Besenhard, J. O.; Hess, M.; Komenda, P. Dimensionally Stable Li-Alloy Electrodes for Secondary Batteries. *Solid State Ionics* **1990**, *40−41*, 525−529.

(10) Wang, J.; Raistrick, I. D.; Huggins, R. A. Behavior of Some Binary Lithium Alloys as Negative Electrodes in Organic Solvent-Based Electrolytes. *J. Electrochem. Soc.* **1986**, *133*, 457−460.

(11) Thacheray, M. M.; Vaughey, J. T.; Johnson, C. S.; Kropf, A. J.; Benedek, R.; Fransson, L. M. L.; Edstrom, K. Structural Considerations of Intermetallic Electrodes for Lithium Batteries. *J. Power Sources* **2003**, *113*, 124−130.

(12) Benedek, R.; Thacheray, M. M. Lithium Reactions with Intermetallic-Compound Electrodes. *J. Power Sources* **2002**, *110*, 406−411.

(13) Wang, F.; Zhao, M.; Song, X. Influence of The Preparation Conditions on the Morphology and Electrochemical Performance of Nano-Sized Cu−Sn Alloy Anodes. *J. Alloys Compd.* **2007**, *439*, 249−253.

(14) Kepler, K. D.; Vaughey, J. T.; Thackeray, M. M. $Li_xCu_6Sn_5$ ($0 < x < 13$): An Intermetallic Insertion Electrode for Rechargeable Lithium Batteries. *Electrochem. Solid-State Lett.* **1999**, *2*, 307−309.

(15) Choi, W.; Lee, J.; Lim, H. S. Electrochemical lithiation reactions of Cu_6Sn_5 and their reaction products. *Electrochem. Commun.* **2004**, *8*, 816−820.

(16) Naille, S.; Bousquet, C. M.; Robert, F.; Morato, F.; Lippens, P.-E.; Fourcade, O. Sn-based intermetallic materials: Performances and mechanisms. *J. Power Sources.* **2007**, *2*, 1091−1094.

(17) Wolfenstine, J.; Campos, S.; Foster, D.; Read, J.; Behl, W. K. Nano-scale Cu_6Sn_5 Anodes. *J. Power Sources* **2002**, *109*, 230−233.

(18) Xue, L.; Fu, Z.; Yao, Y.; Huang, T.; Yu, A. Three-Dimensional Porous Sn−Cu Alloy Anode for Lithium-Ion Batteries. *Electrochim. Acta* **2010**, *55*, 7310−7314.

(19) Chiu, K. F.; Lin, K. M.; Lin, H. C.; Chen, W. Y.; Shieh, D. T. Structural Evolution and Electrochemical Performance of Sputter-Deposited Cu_6Sn_5 Thin-Film Anodes. *J. Electrochem. Soc.* **2007**, *154*, A433−A437.

(20) Bazin, L.; Mitra, S.; Taberna, P. L.; Poizot, P.; Gressier, M.; Menu, M. J.; Barnabé, A.; Simon, P.; Trascon, J. M. High Rate Capability Pure Sn-Based Nano-Architectured Electrode Assembly for Rechargeable Lithium Batteries. *J.Power Sources* **2009**, *188*, 578−582.

(21) Chen, J.; Yang, L.; Fang, S.; Hirano, S.; Tachibana, K. Three-Dimensional Core−Shell $Cu@Cu_6Sn_5$ Nanowires as the Anode Material for Lithium Ion Batteries. *J. Power Sources* **2012**, *199*, 341−345.

(22) Tian, M.; Wang, W.; Lee, S. H.; Lee, Y. C.; Yang, R. Enhancing Ni−Sn Nanowire Lithium-Ion Anode Performance by Tailoring Active/Inactive Material Interfaces. *J. Power Sources* **2011**, *196*, 10207−10212.

(23) Karabacak, T.; Wang, G. C.; Lu, T. M. Enhanced Layer Coverage of Thin Films by Oblique Angle Deposition. *Mater. Res. Soc. Symp. Proc.* **2005**, *859 E*, JJ9.5.1−6.

(24) Hu, R. Z.; Zhang, Y.; Zhu, M. Microstructure and Electrochemical Properties of Electron-Beam Deposited Sn−Cu Thin Film Anodes for Thin Film Lithium Ion Batteries. *Electrochim. Acta* **2008**, *53*, 3377−3385.

(25) Pu, W.; He, X.; Ren, J.; Wan, C.; Jiang, C. Electrodeposition of Sn−Cu Alloy Anodes for Lithium Batteries. *Electrochim. Acta* **2005**, *50*, 4140−4145.

(26) Jensen, M. O.; Brett, M. J. Porosity Engineering in Glancing Angle Deposition Thin Films. *Appl. Phys. A: Mater. Sci. Process.* **2005**, *80*, 763−768.

(27) Robbie, K.; Brett, M. J. Sculptured Thin Films and Glancing Angle Deposition: Growth Mechanics and Applications. *J. Vac. Sci. Technol. A* **1997**, *15*, 1460−1465.

(28) Li, J.; Swiatowska, J.; Seyeux, A.; Huang, L. Maurice, V., Sun,S.; Marcus, P. XPS and ToF-SIMS study of Sn-Co Alloy Thin Films as Anode for Lithium Ion Battery. *J. Power Sources* **2010**, *24*, 8251−8257.

(29) Chen, Y. C.; Chen, J. M.; Huang, Y. H.; Lee, Y. R.; Shih, H. C. Size Effect Of Tin Oxide Nanoparticles On High Capacity Lithium Battery Anode Materials. *Surf. Coat. Technol.* **2007**, *202*, 1313−1318.

(30) Nguyen, C.; Woo, S. W.; Song, S. W. Understanding the Interfacial Processes at Silicon−Copper Electrodes in Ionic Liquid Battery Electrolyte. *J. Phys. Chem. C* **2012**, *116*, 14764−14771.

(31) Shieh, D. T.; Yin, J.; Yamamoto, K.; Wada, M.; Tanase, S.; Sakai, T. Surface Characterization on Lithium Insertion/Deinsertion Process for Sputter-Deposited AgSn Thin-Film Electrodes by XPS. *J. Electrochem. Soc.* **2006**, *153*, A106−112.
(32) Nie, M.; Abraham, D. P.; Seo, D. M.; Chen, Y.; Bose, A.; Lucht, B. L. Role of Solution Structure in Solid Electrolyte Interphase Formation on Graphite with $LiPF_6$ in Propylene Carbonate. *J. Phys. Chem. C* **2013**, *117* (48), 25381−25389.
(33) Hu, R. Z.; Zeng, M. Q.; Zhu, M. Cyclic Durable High-Capacity Sn/Cu_6Sn_5 Composite Thin Film Anodes for Lithium Ion Batteries Prepared by Electron-Beam Evaporation Deposition. *Electrochim. Acta* **2009**, *54*, 2843−2850.
(34) Xia, Y.; Sakai, T.; Fujieda, T.; Wada, M.; Yoshinaga, H. Flake Cu-Sn Alloys as Negative Electrode Materials for Rechargeable Lithium Batteries. *J. Electrochem. Soc.* **2001**, *5*, A471−481.
(35) Kepler, K. D.; Vaughey, J. T.; Thackeray, M. M. Copper-Tin Anodes for Rechargeable Lithium Batteries: An Exemple of the Matrix effect in an Intermetallic System. *J.Power Sources* **1999**, *81−82*, 383−387.
(36) Park, J. W.; Eom, J.; Kwon, H. Charge-Discharge Characteristics of a Layered-Structure Electroplated Cu/Sn anode for Li-Ion Batteries. *Electrochim. Acta* **2010**, *5*, 1825−1828.